

# Concerted or Stepwise Mechanism? CASPT2 and LC-TDDFT Study of the Excited-State Double Proton Transfer in the 7-Azaindole Dimer

Xue-fang Yu, Shohei Yamazaki, and Tetsuya Taketsugu\*

Division of Chemistry, Graduate School of Science, Hokkaido University, Sapporo 060-0810, Japan

 Supporting Information

**ABSTRACT:** Excited-state double proton transfer (ESDPT) in the 7-azaindole dimer is investigated using the complete active space second-order perturbation theory (CASPT2) method and the long-range corrected time-dependent density functional theory (LC-TDDFT) method. These methods are employed for geometry optimizations as well as single-point energy calculations of the excited-state potential energy profiles along the reaction paths. It is shown that three main reaction routes involving double proton transfer exist. In the first route, the ESDPT reaction takes place in the locally excited state through a single transition state following the concerted mechanism in which each proton-transfer process occurs simultaneously without forming any stable zwitterionic intermediate. The concerted ESDPT reaction is found to proceed asynchronously in  $C_s$  symmetry rather than synchronously in  $C_{2h}$  symmetry. In the second and third routes, on the other hand, the ESDPT reaction takes place following the stepwise mechanism in which each proton-transfer process occurs sequentially forming a neutral intermediate in the charge-transfer state. The calculated energy profiles of the three routes exhibit a lower barrier in the first route than in the other routes, suggesting that the ESDPT in the gas phase is likely to follow the asynchronous concerted mechanism at the lowest excitation energy.

## 1. INTRODUCTION

Proton-transfer reactions play essential roles in physics, chemistry, and biology.<sup>1–3</sup> Among them, excited-state double proton transfer (ESDPT) in the 7-azaindole (7AI) dimer has been receiving particular attention (see ref 4 for a recent review), because this process can be taken as a model of the photoinduced mutation in DNA base pairs. Thus this process has been intensively studied experimentally<sup>4–38</sup> and theoretically<sup>22,29,34,39–50</sup> for more than 40 years. Through these studies, one major question has been put forward: Does the ESDPT follow a concerted mechanism or a stepwise mechanism? Figure 1 shows schematic pictures of the mechanisms of the ESDPT in the 7AI dimer from the normal dimer (ND) to the tautomer dimer (TD), derived from previous studies. In the concerted mechanism (Figure 1a), two protons are simultaneously transferred through a single transition state, without forming a stable intermediate for the single proton-transferred (SPT) component. The concerted DPT does not necessarily require synchronous motion of the two protons in which molecular structure of the dimer strictly keeps  $C_{2h}$  symmetry, but it can take asynchronous motion in which the two protons are transferred cooperatively in  $C_s$  symmetry, breaking the  $C_{2h}$  structure of the dimer.<sup>36</sup> In the stepwise mechanism (Figure 1b), on the other hand, a stable intermediate is formed by the first SPT from ND, followed by the second SPT to TD. This intermediate can have either a zwitterionic character or a neutral character.<sup>42,43,46,49</sup> A zwitterionic intermediate is formed when the first SPT occurs in the locally excited (LE) state, while a neutral intermediate is formed when the first SPT occurs with transition to the charge-transfer (CT) state.

The mechanism of ESDPT in the 7AI dimer has been extensively discussed among several experimental groups, but it is still in controversy. Zewail and co-workers<sup>17,19,28,37</sup> proposed the stepwise mechanism based on time-resolved spectra of the

7AI dimer in nonpolar and polar solvent as well as in the gas phase. The authors observed biexponential decay in the electronic spectra and assigned the faster and slower components of the decay to the first and second SPTs of the stepwise ESDPT, respectively. The decay time was found to strongly depend on solvent polarity, which was explained by the existence of a zwitterionic intermediate.<sup>37</sup> Castleman and co-workers<sup>20,23,24</sup> supported the stepwise mechanism using the Coulomb explosion technique. On the other hand, Takeuchi and Tahara<sup>18,21,26,36</sup> presented evidence of the concerted mechanism by examining the time-resolved fluorescence decay and its dependency on the excitation wavelength for the 7AI dimer in nonpolar solvent. These authors also detected the biexponential decay of fluorescence in ND as Zewail and co-workers did. However, they attributed the faster and slower components to internal conversion from the  $S_2$  to  $S_1$  state and the concerted ESDPT in the  $S_1$  state, respectively, because the faster component was not observed at the lowest excitation energy. Sekiya, Sakota, and co-workers<sup>4,28,31–33,35</sup> supported the concerted mechanism in terms of frequency- and time-resolved electronic spectra of the isolated 7AI dimer and its deuterated compounds. In particular, they concluded that the biexponential decay of fluorescence is not a proper evidence of the stepwise mechanism by using picosecond time-resolved resonance-enhanced multiphoton ionization (REMPI) spectroscopy.

Meanwhile, a large number of theoretical studies<sup>22,29,34,39–50</sup> on the ESDPT in the 7AI dimer have been reported using semiempirical methods, ab initio methods, and density functional theory (DFT), but they have also exhibited different mechanisms. Several authors<sup>22,42,43,46</sup> proposed the stepwise mechanism

**Received:** January 8, 2011

**Published:** March 16, 2011

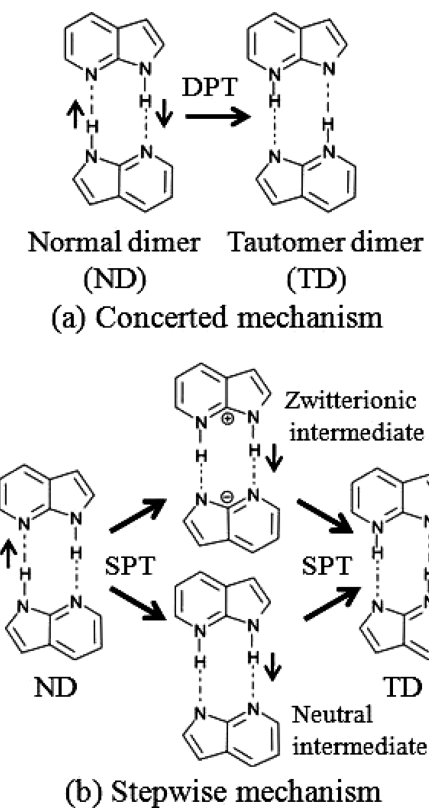


Figure 1. Two mechanisms of ESDPT in the 7AI dimer: (a) concerted mechanism and (b) stepwise mechanism.

via a zwitterionic intermediate or a neutral intermediate on the basis of the excited-state geometry optimizations with the configuration interaction singles (CIS) method. On the other hand, Catalán, Kasha, and co-workers<sup>29,34,44,45,47</sup> concluded that the ESDPT follows the concerted mechanism in which the reaction path conserves  $C_{2h}$  symmetry by using the DFT and time-dependent DFT (TDDFT) methods with hybrid B3LYP functional. In 2006, Serrano-Andrés and Merchán<sup>49</sup> proposed the reaction paths of the ESDPT supporting the stepwise mechanism based on the single-point energy calculations with the complete active space second-order perturbation theory (CASPT2) method at the geometries optimized with the complete active space self-consistent-field (CASSCF) method. The authors reported that the stepwise reaction path through a zwitterionic intermediate should be more favorable than the concerted pathway in  $C_{2h}$  symmetry. However, the stepwise pathway with an intermediate minimum could not be reproduced in CASPT2 calculations by Nanbu and Sekiya (see ref 4). In addition, Ando and Kato<sup>50</sup> presented the reaction surface of the ESDPT supporting the concerted mechanism with very similar procedure as Serrano-Andrés and Merchán used: single-point energy calculations with the multireference second-order Møller–Plesset (MRMP2) method for the geometries optimized with the CASSCF method.

The present work aims to clarify the mechanism of the ESDPT reaction in the 7AI dimer thoroughly by means of more accurate ab initio and DFT calculations. For this purpose, the CASPT2 method<sup>51,52</sup> and the long-range corrected TDDFT (LC-TDDFT) method<sup>53,54</sup> are employed for geometry optimizations as well as single-point energy calculations along the excited-state reaction paths. Potential energy profiles are

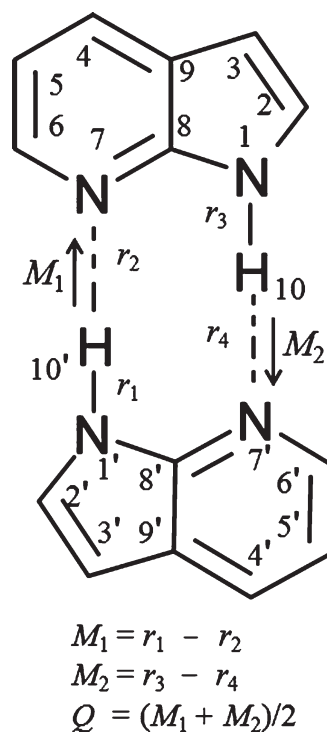


Figure 2. Definition of significant coordinates of ESDPT in the 7AI dimer. Labels for atoms are also given.

calculated for the ESDPT in the LE state as well as in the CT state in order to elucidate which mechanism in Figure 1 is the most favorable. Two major improvements in our approaches compared with other theoretical studies should be emphasized. First, the CASPT2 method is employed not only for single-point energy calculations but also for geometry optimizations in the excited states to take into account the dynamic electron correlation effect. Geometry optimizations with the CIS or CASSCF method may give less accurate structures due to the lack of dynamic correlation.<sup>55</sup> In the present work, analytical energy gradient<sup>52</sup> is used for the CASPT2 geometry optimizations. Second, the long-range correction (LC) scheme is employed in TDDFT calculations. It is well-known that the TDDFT method with conventional exchange–correlation functionals, such as B3LYP, considerably underestimates the energies of CT states due to the lacking of nonlocal electron–electron exchange interaction.<sup>56,57</sup> The LC scheme can overcome this disadvantage by modifying the long-range electron–electron interaction part of exchange functional by using the Hartree–Fock exchange integral. The reaction paths calculated at the CASPT2 and LC-TDDFT levels are expected to give a conclusive description of the ESDPT mechanism in the 7AI dimer.

## 2. COMPUTATIONAL DETAILS

Equilibrium geometries of ND and TD structures of the 7AI dimer in the ground state, referred to as ND<sub>SO</sub> and TD<sub>SO</sub>, respectively, and the geometry of the transition state between them, referred to as TS<sub>SO</sub>, were optimized by the Møller–Plesset second-order perturbation (MP2) method. For geometry optimization in the excited states, the CASPT2<sup>51,52</sup> and LC-TDDFT<sup>53,54</sup> methods were used. In the LC-TDDFT calculations, we employed the Becke 1988 exchange<sup>58</sup> and Lee–Yang–Parr correlation<sup>59,60</sup> functional

with the long-range correction (LC-BLYP functional). Equilibrium geometries in the lowest singlet LE state of ND and TD structures, referred to as  $\text{ND}_{\text{LE}}$  and  $\text{TD}_{\text{LE}}$ , respectively, as well as the reaction path between  $\text{ND}_{\text{LE}}$  and  $\text{TD}_{\text{LE}}$  were determined by both the CASPT2 and LC-BLYP methods. The transition state between  $\text{ND}_{\text{LE}}$  and  $\text{TD}_{\text{LE}}$  in the LE state (referred to as  $\text{TS}_{\text{LE}}$ ), minimum in the lowest singlet CT state (referred to as  $\text{IN}_{\text{CT}}$ ), and the transition state between the LE and CT minima (referred to as  $\text{TS}_{\text{CT}}$ ) were optimized by the LC-BLYP method. The geometry optimizations above were performed in  $C_s$  symmetry. Geometry optimizations with  $C_{2h}$  symmetry constraint were also performed by the LC-BLYP method for the minima of ND and TD structures in the first singlet excited state, referred to as  $\text{ND}_{\text{S}1}(C_{2h})$  and  $\text{TD}_{\text{S}1}(C_{2h})$ , respectively, and the transition state between them, referred to as  $\text{TS}_{\text{S}1}(C_{2h})$ . For the stationary points optimized with the MP2 method or the LC-BLYP method, normal-mode analysis was performed at the same computational level to check whether they are a minimum, a transition state, or a saddle point of higher order as well as to calculate the zero-point energy. Normal-mode analysis at the CASPT2 level could not be performed due to a huge computational cost.

Several reaction coordinates were introduced to describe a double proton transfer (DPT) process; see Figure 2. The coordinates  $M_1 = r_1 - r_2$  and  $M_2 = r_3 - r_4$ , where  $r_1$ ,  $r_2$ ,  $r_3$ , and  $r_4$  are the length of N1'-H10', N7-H10', N1-H10, and N7'-H10 bond, respectively, characterize the transfer of each proton in N-H $\cdots$ N hydrogen bonds. The coordinate  $Q$  is defined by the average of  $M_1$  and  $M_2$ :  $Q = (M_1 + M_2)/2$ . The energy profiles along the reaction path from  $\text{ND}_{\text{LE}}$  to  $\text{TD}_{\text{LE}}$  were calculated as a function of the proton-transfer coordinate  $Q$ , in which the value of  $Q$  was fixed, and all other internal coordinates were optimized along the reaction path.

In geometry optimization at the CASPT2 level, the underlying state-averaged (SA) CASSCF wave function was generated with the active space of four electrons in four  $\pi$  orbitals, which are all localized on one of the monomers, and was averaged over the lowest three singlet states with equal weights (referred to as SA3-CASSCF(4,4)). Then single and double excitations from the reference space were taken into account by a perturbational treatment (referred to as CASPT2(4,4)) where 34 double-occupied orbitals were frozen to reduce the computational cost. A level shift with the parameter of 0.3 was employed for the CASPT2(4,4) calculations.<sup>61</sup>

For the CASPT2(4,4)-optimized geometries, single-point energies of the lowest 6 singlet states were calculated at the internally contracted CASPT2(12,12) level with 18 frozen core orbitals (1s orbitals of C and N atoms) and a level shift of 0.3, following SA6-CASSCF(12,12) calculations. The (12,12) active space includes 6  $\pi$  orbitals of each monomer. The CASPT2-(12,12) method was also used for calculation of the vertical excitation energies at  $\text{ND}_{\text{S}0}$ .

Along the reaction path in the LE state optimized with the LC-BLYP method, energies of the lowest 20 singlet excited states were calculated at the same level. To examine the effect of the LC scheme, the excited-state energies were also calculated by the conventional TDDFT method with the pure BLYP functional<sup>58–60</sup> and hybrid B3LYP functional.<sup>62–64</sup>

The Sapporo-DZP basis set<sup>65–68</sup> was used for the calculations in the present work. One exception is for geometry optimization at the CASPT2(4,4) level along the reaction path, where polarization basis functions for hydrogen atoms other than the transferred ones were eliminated from Sapporo-DZP. CASPT2

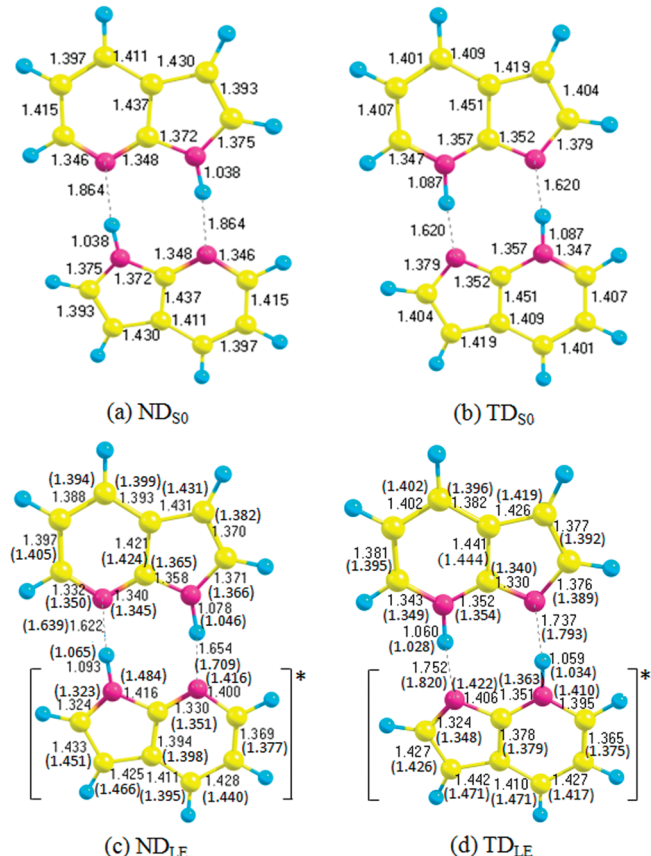


**Figure 3.** Equilibrium geometries of the 7AI dimer in the ground state, optimized at the MP2 level: (a)  $\text{ND}_{\text{S}0}$  and (b)  $\text{TD}_{\text{S}0}$  and minimum-energy geometries of the 7AI dimer in the lowest LE state, optimized at the LC-BLYP level: (c)  $\text{ND}_{\text{LE}}$  and (d)  $\text{TD}_{\text{LE}}$ . In panels c and d, bond lengths obtained by CASPT2(4,4) optimizations are given in parentheses. Bond lengths are in angstroms. Monomer in [ \* ] indicates monomer-e.

calculations were performed with MOLPRO 2008.1,<sup>69</sup> while TDDFT calculations were performed with GAMESS.<sup>70</sup>

### 3. RESULTS AND DISCUSSION

#### 3.1. Equilibrium Geometries and Excitation Energies.

Figure 3 shows equilibrium structures in the ground and LE states, optimized by the MP2 method and the LC-TDDFT (LC-BLYP) method, respectively. For the LE minima, bond lengths obtained by the CASPT2(4,4) optimization are given in parentheses. The MP2-optimized geometries of  $\text{ND}_{\text{S}0}$  and  $\text{TD}_{\text{S}0}$  (Figure 3a and b, respectively) as well as  $\text{TS}_{\text{S}0}$  (see the Supporting Information) belong to  $C_{2h}$  point group. The activation barrier from  $\text{ND}_{\text{S}0}$  side is calculated as 15.0 kcal/mol, while the barrier from  $\text{TD}_{\text{S}0}$  side is calculated as 0.9 kcal/mol. These barrier heights indicate that the reverse DPT in the ground state from  $\text{TD}_{\text{S}0}$  to  $\text{ND}_{\text{S}0}$  is very favorable and thus support the spectroscopic observation for TD in the ground state.<sup>71</sup>

As shown in Figure 3c and d, equilibrium structures in the lowest LE state ( $\text{ND}_{\text{LE}}$  and  $\text{TD}_{\text{LE}}$ ) optimized at the LC-BLYP and CASPT2(4,4) levels are in  $C_s$  symmetry, that is, the two monomers of the 7AI dimer exhibit different structures. The excitation to the  $S_1$  state at  $\text{ND}_{\text{LE}}$  and  $\text{TD}_{\text{LE}}$  is localized on one of the monomers. The excited monomer is referred to as monomer-e

(indicated by bracket and star in Figure 3c and d). The geometry of monomer-e is largely deviated by excitation, while the other monomer almost keeps the ground-state geometry (referred to as monomer-g). Thus the structure of the 7AI dimer deviates from  $C_{2h}$  symmetry at ND<sub>LE</sub> and TD<sub>LE</sub>. In the CASPT2(4,4) optimization, the four active orbitals for the underlying SA3-CASSCF(4,4) wave function are selected to be localized on monomer-e, see Figure 4. The active orbitals correspond to the highest occupied molecular orbital (HOMO), HOMO-1, the lowest unoccupied molecular orbital (LUMO), and LUMO+1 of monomer-e. In SA-CASSCF calculations, the ground and two LE states, the latter of which correspond to the  $^1\text{L}_a$  and  $^1\text{L}_b$  excitations<sup>72</sup> localized on monomer-e, are averaged with equal weights. The  $^1\text{L}_a$  excitation is mainly composed by configuration

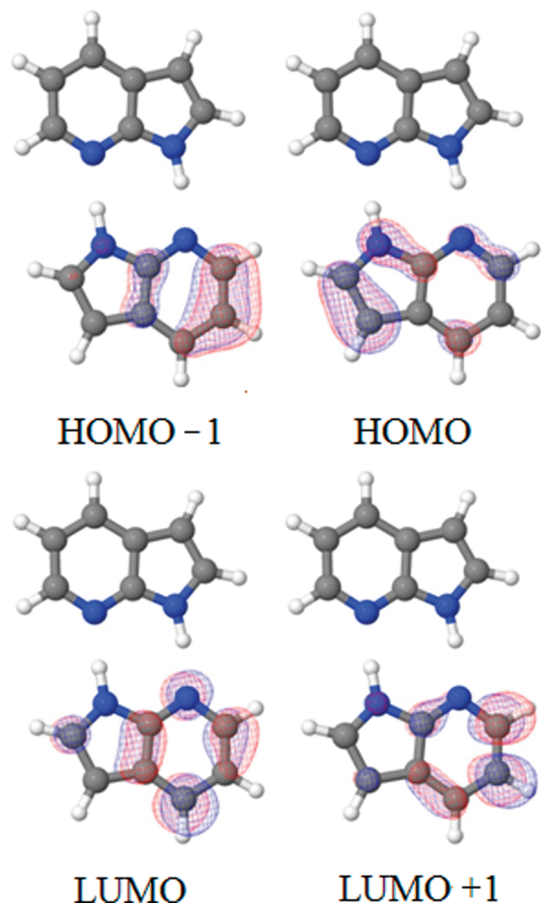


Figure 4. Active orbitals in CASPT2(4,4) calculations at ND<sub>LE</sub>.

for the excitation from HOMO to LUMO, while the  $^1\text{L}_b$  excitation is mainly composed by configurations for the excitation from HOMO-1 to LUMO and the excitation from HOMO to LUMO+1. The LE states included in the SA3-CASSCF(4,4) calculations are referred to as  $\text{S}_0-^1\text{L}_a$  and  $\text{S}_0-^1\text{L}_b$ , where the label  $\text{S}_0-^1\text{L}_a$  ( $\text{S}_0-^1\text{L}_b$ ) means that monomer-g is in the ground state, while monomer-e is in the  $^1\text{L}_a$  ( $^1\text{L}_b$ ) state. The lowest LE state is the  $\text{S}_0-^1\text{L}_a$  state at ND<sub>LE</sub> as well as at TD<sub>LE</sub> optimized with the CASPT2(4,4) method. This is also true for ND<sub>LE</sub> and TD<sub>LE</sub> optimized with the LC-BLYP method.

Table 1 shows excitation and emission energies related to the ESDPT process in the 7AI dimer, including the vertical excitation energies for the lowest two singlet excited states at ND<sub>S0</sub>, the adiabatic excitation energies for the lowest LE state of ND, and the vertical emission energies for the lowest LE state at ND<sub>LE</sub> and TD<sub>LE</sub>, calculated at the LC-BLYP and the CASPT2(12,12) levels. For the vertical excitation of the 7AI dimer in  $C_{2h}$  symmetry, the lowest two excited states are  $^1\text{B}_u$  and  $^2\text{A}_g$ , and they are nearly degenerate at both the LC-BLYP and CASPT2 levels. The  $^1\text{B}_u$  and  $^2\text{A}_g$  states are optically allowed and forbidden, respectively, in  $C_{2h}$  symmetry. These states correspond to linear combinations of the configurations for the  $^1\text{L}_a$  local excitation on each monomer, i.e.,  $\text{S}_0-^1\text{L}_a$  and  $^1\text{L}_a-\text{S}_0$ . These findings are consistent with the results of recent theoretical studies.<sup>49,73</sup> When the molecular structure is relaxed from  $C_{2h}$  to  $C_s$  symmetry, the excitation is localized in the  $\text{S}_0-^1\text{L}_a$  and  $^1\text{L}_a-\text{S}_0$  states, and the first excited state is thus stabilized.

The calculated excitation and emission energies in Table 1 qualitatively agree with experimental values. The vertical excitation energy of the  $^1\text{B}_u$  state is 4.74 eV at the LC-BLYP level and 3.98 eV at the CASPT2 level, corresponding to the wavelengths of 262 and 312 nm, respectively. These values are consistent with absorption spectra of ND in nonpolar solvent.<sup>19,36,38</sup> The  $^2\text{A}_g$  state exhibits similar values of vertical excitation energy: 4.76 and 3.96 eV (261 and 313 nm) at the LC-BLYP and CASPT2 levels, respectively. Adiabatic excitation energy of ND is 4.30 eV (288 nm) at the LC-BLYP level and 3.93 eV (316 nm) at the CASPT2 level. The adiabatic excitation energy at the LC-BLYP level is corrected to be 4.16 eV (298 nm) when the zero-point energies of ND<sub>S0</sub> and ND<sub>LE</sub> (calculated with the MP2 and LC-BLYP methods, respectively) are included. The calculated adiabatic excitation energies can be compared with the ionization spectra for jet-cooled ND (4.00 eV, 310 nm).<sup>12,15</sup> Vertical emission energies for ND<sub>LE</sub> and TD<sub>LE</sub> are 3.93 and 2.97 eV (316 and 418 nm) at the CASPT2 level, while they are 3.63 and 2.02 eV (342 and 614 nm) at the LC-BLYP level. These results are also consistent with the fluorescence spectra of the 7AI dimer in nonpolar solvent with respect to the position of the peaks

**Table 1. Vertical Excitation Energy, Adiabatic Excitation Energy, and Vertical Emission Energy Calculated at the LC-BLYP and CASPT2(12,12) Levels (eV)**

method	vertical excitation		ND <sub>LE</sub> ← ND <sub>S0</sub>	vertical emission	
	ND <sub>S0</sub> ( $^1\text{B}_u$ )	ND <sub>S0</sub> ( $^2\text{A}_g$ )		ND <sub>LE</sub>	TD <sub>LE</sub>
LC-BLYP	4.74	4.76	4.30 (4.16) <sup>a</sup>	3.93	2.97
CASPT2(12,12)	3.98	3.96	3.93	3.63	2.02
expt	4.32, <sup>b</sup> 4.34 <sup>c</sup>		4.00 <sup>d</sup>	3.54 <sup>e</sup>	2.58, <sup>e</sup> 2.53 <sup>f</sup>

<sup>a</sup>Zero-point energy correction is implemented. <sup>b</sup>Absorption band maximum in hexane.<sup>36</sup> <sup>c</sup>Absorption band maximum in 3-methylpentane and ethylcyclohexane.<sup>38</sup> <sup>d</sup>Band origins for jet-cooled ND in ionization spectrum.<sup>12,15</sup> <sup>e</sup>Fluorescence band maximum in 3-methylpentane and ethylcyclohexane.<sup>38</sup> <sup>f</sup>Fluorescence band maximum in hexane.<sup>36</sup>

corresponding to the emission from ND and TD.<sup>5,19,36,38</sup> The transition energies at the CASPT2 level tend to be lower than the experimental results, while the transition energies at the LC-BLYP level are a little higher than the experimental values. The excitation and emission energies given in Table 1 are also consistent with those calculated in previous theoretical studies.<sup>34,49</sup>

Geometry optimization was also performed for ND and TD structures in the lowest excited state with constraint of  $C_{2h}$  symmetry [ND<sub>S1</sub>( $C_{2h}$ ) and TD<sub>S1</sub>( $C_{2h}$ ), respectively] at the LC-BLYP level. The resulting structures are shown in the Supporting Information. These stationary points were found to be higher in energy by 4.6 and 5.3 kcal/mol than ND<sub>LE</sub> and TD<sub>LE</sub>, respectively, in  $C_s$  symmetry. From the normal-mode analysis, both ND<sub>S1</sub>( $C_{2h}$ ) and TD<sub>S1</sub>( $C_{2h}$ ) are shown to have one imaginary frequency mode of  $b_u$  irreducible representation which breaks  $C_{2h}$  symmetry. This means that ND<sub>S1</sub>( $C_{2h}$ ) and TD<sub>S1</sub>( $C_{2h}$ ) correspond to the transition states in  $C_s$  symmetry connecting two ND<sub>LE</sub> structures ( $S_0-^1L_a$  and  $^1L_a-S_0$ ) and two TD<sub>LE</sub> structures ( $S_0-^1L_a$  and  $^1L_a-S_0$ ), respectively. The double-minimum feature of the potential energy surface is consistent with the weak coupling case of Frenkel-type exciton model discussed in ref 4.

From Figure 3, one can see that the bond lengths of the hydrogen-bonded N–H···N part are quite different between the  $S_0$  minima and the LE minima. In particular, the N···H distances of ND ( $r_2$  and  $r_4$ , see Figure 2) are considerably shortened by excitation. With respect to ND<sub>S0</sub> optimized at the MP2 level and ND<sub>LE</sub> optimized at the LC-BLYP level, the N···H distances  $r_2$  and  $r_4$  vary from 1.864 to 1.622 Å and 1.864 to 1.654 Å, respectively. These findings suggest that the strength of N–H···N hydrogen bonds of ND is enhanced in the excited state compared to the ground state. The DPT reaction from ND is therefore expected to become facilitated by the strengthened intermolecular hydrogen bonds in the LE state.

Compared to the CIS- and CASSCF-optimized geometries in previous studies,<sup>46,49</sup> much shorter N···H bond lengths have been exhibited for the LE minimum geometries optimized by the LC-BLYP or CASPT2 method; taking the N7···H10' distance of ND<sub>LE</sub> for example, the distance calculated at the LC-BLYP level (CASPT2 level) is shorter by 0.486 Å (0.469 Å) than the CASSCF-optimized value (2.108 Å).<sup>49</sup> It is also much shorter than CIS-optimized N···H distance of ca. 2.0 Å.<sup>42,46</sup> This difference is caused by the limitation of the CIS and CASSCF methods which both do not take into account dynamic electron correlation. The  $S_0$  minima optimized at the MP2 level also exhibit much shorter N···H distance than at the Hartree–Fock level and CASSCF level.<sup>42,49</sup> The  $S_0$  and LE minima optimized at the B3LYP level<sup>34,46</sup> exhibit smaller difference of the N···H distance from those optimized at the MP2, LC-BLYP, and CASPT2 levels (difference is less than 0.14 Å).

For ND<sub>LE</sub>, one can also notice that some bond lengths on the rings of monomer-e optimized with the LC-BLYP and CASPT2 methods are considerably different from those optimized with the CASSCF method.<sup>49</sup> In our LC-BLYP and CASPT2 calculations, the  $^1L_a$  (HOMO → LUMO) local excitation of monomer-e induces significantly longer bond lengths of N1'–C8' and C2'–C3' as well as shorter bond lengths of C8'–C9' and C6'–C5' compared with the corresponding bonds of monomer-g (see Figure 3c). The longer bond lengths reflect the reduction of bonding character by excitation from HOMO, while the shorter bond lengths reflect the enhancement of bonding

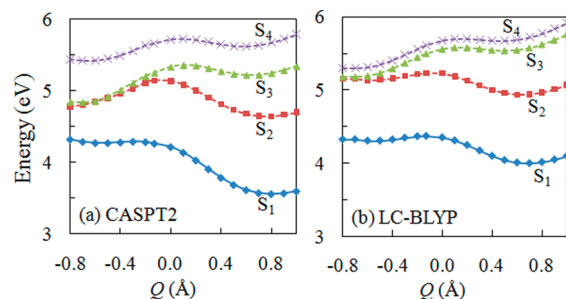


**Figure 5.** Potential energy profiles of the lowest four excited states of the 7AI dimer as functions of the reaction coordinate  $Q$ , calculated at the (a) CASPT2(12,12) and (b) LC-BLYP levels. Reaction paths in panels a and b are optimized for the lowest LE ( $S_1$ ) state with the CASPT2(4,4) and LC-BLYP methods, respectively. Ground-state energy of ND<sub>S0</sub> is taken as zero. Full line with filled diamonds indicates energies of  $S_1$  state whose geometries are optimized. Dashed lines show energies of higher LE states at the  $S_1$ -optimized geometries.

character by excitation to LUMO (see Figure 4). The C1'–C2' bond of monomer-e is also much shorter than C1–C2 bond of monomer-g, reflecting the reduction of antibonding character by excitation from HOMO. In the previous CASSCF calculation, on the other hand, C8'–C9' and C6'–C5' bond lengths of monomer-e are longer than the corresponding bonds of monomer-g, which may reflect the reduction of bonding character by excitation from HOMO-1 or excitation to LUMO+1. The difference suggests that the configuration of  $^1L_b$  local excitation has significant contribution to the  $S_1$  state of ND<sub>LE</sub> optimized at the CASSCF level. For TD<sub>LE</sub>, our LC-BLYP and CASPT2 calculations as well as the previous CASSCF calculation predict the  $^1L_a$  local excitation of monomer-e, exhibiting longer bond lengths of N1'–C8' and C2'–C3' by excitation from HOMO and shorter bond lengths of C8'–C9' and C6'–C5' by excitation to LUMO (see Figure 3d).

### 3.2. Reaction Path of ESDPT in the Locally Excited State.

To understand the ESDPT mechanism of the 7AI dimer in the lowest LE state, the reaction path starting from ND<sub>LE</sub> to TD<sub>LE</sub> was determined at the CASPT2(4,4) level as well as at the LC-BLYP level along the reaction coordinate  $Q$  defined in Figure 2. Once the reaction path was determined, energies of the first and higher excited states were calculated along the CASPT2 and LC-BLYP reaction paths by the CASPT2(12,12) (for the lowest five excited states) and LC-BLYP (for the lowest 20 excited states) methods, respectively. Figure 5 shows the calculated energy profiles in the lowest four excited states where the energy of ND<sub>S0</sub> is taken as zero in each figure. At both the CASPT2 and LC-BLYP levels, the first excited state is dominated by the LE configuration labeled as  $S_0-^1L_a$ , where monomer-g is kept in the ground state and monomer-e is in the  $^1L_a$  excited state. At the LC-BLYP level, the second excited state corresponds to the  $^1L_a-S_0$  state, where monomer-g is locally excited to the  $^1L_a$  state and monomer-e is in the ground state. The third and fourth excited states correspond to the local excitation to the  $^1L_b$  states of monomer-e and monomer-g, i.e., the  $S_0-^1L_b$  and  $^1L_b-S_0$  states, respectively. The fifth and higher excited states include  $^1n-\pi^*$  states corresponding to the excitation from the lone-pair orbital of the N atoms as well as CT states where an electron is transferred between the two monomers. At the CASPT2 level, the second, third, and fourth excited states contain contributions of several electronic configurations including  $S_0-^1L_a$ ,  $^1L_a-S_0$ ,

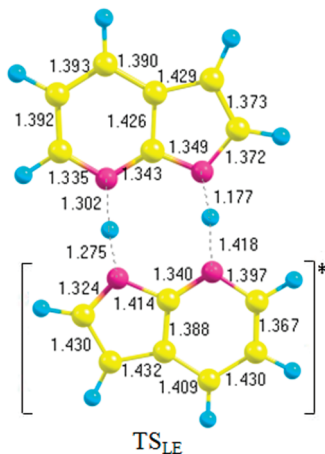


**Figure 6.** Geometry of transition state on DPT reaction path of the 7AI dimer in the lowest LE state ( $TS_{LE}$ ), optimized at the LC-BLYP level. Bond lengths are in angstroms. Monomer in  $[ ]^*$  indicates monomer-e.

$S_0 - ^1L_b$ , and  $^1L_b - S_0$ . The fifth excited state is described by a doubly excited configuration which can be labeled as  $^1L_a - ^1L_a$ , where both monomers are simultaneously excited to the  $^1L_a$  state. It should be emphasized that the lowest four excited states along the reaction path are dominated by LE excitations at both CASPT2 and LC-BLYP levels and that no significant contribution of CT excitations is found. It is also worthy to mention that the LC-BLYP method reproduces the CASPT2 energy profiles in certain extent for the four LE states.

As shown in Figure 5, for the lowest LE state at both the CASPT2 and LC-BLYP levels, only one energy maximum has been found along the ESDPT reaction path connecting  $ND_{LE}$  and  $TD_{LE}$ , and no minimum for a stable zwitterionic intermediate could be located. The CASPT2 and LC-BLYP methods thus predict that the ESDPT in the LE state follows the concerted mechanism. Both methods show that activation barrier is very low for the concerted ESDPT from  $ND_{LE}$  to  $TD_{LE}$ . At the LC-BLYP level, the transition state  $TS_{LE}$  ( $Q = -0.134 \text{ \AA}$ ) between  $ND_{LE}$  ( $Q = -0.553 \text{ \AA}$ ) and  $TD_{LE}$  ( $Q = 0.685 \text{ \AA}$ ) is located 1.5 kcal/mol (0.07 eV) higher in energy than  $ND_{LE}$ . When the zero-point correction is applied under the harmonic approximation,  $TS_{LE}$  is 1.9 kcal/mol (0.08 eV) lower in energy than  $ND_{LE}$ . This result suggests that the concerted ESDPT from  $ND_{LE}$  through  $TS_{LE}$  can proceed very efficiently. Figure 6 shows the optimized structure of  $TS_{LE}$ . The intrinsic reaction coordinate (IRC) calculations starting with  $TS_{LE}$  were also performed at the LC-BLYP level, which have confirmed that  $ND_{LE}$  and  $TD_{LE}$  are connected by the reaction path through  $TS_{LE}$ . Meanwhile, optimization of the transition-state geometry at the CASPT2 level could not be completed due to a huge computational cost. Nevertheless, the CASPT2 energy profile in Figure 5a shows a smaller energy barrier of 0.5 kcal/mol (0.02 eV) at  $Q = -0.3 \text{ \AA}$  between  $ND_{LE}$  ( $Q = -0.5 \text{ \AA}$ ) and  $TD_{LE}$  ( $Q = 0.8 \text{ \AA}$ ). The energy of  $TD_{LE}$  is calculated to be 16.4 kcal/mol (0.71 eV) and 7.0 kcal/mol (0.31 eV) lower than  $ND_{LE}$  at the CASPT2 and LC-BLYP levels, respectively, suggesting that the ESDPT process is exothermic.

The  $TS_{LE}$  geometry optimized at the LC-BLYP level in Figure 6 exhibits that the proton at the  $N1' - H10' \cdots N7$  hydrogen bond is located almost in the middle of  $N1'$  and  $N7$  atoms ( $r_1 = 1.275 \text{ \AA}$ ,  $r_2 = 1.302 \text{ \AA}$ ,  $M_1 = -0.027 \text{ \AA}$ ), while the

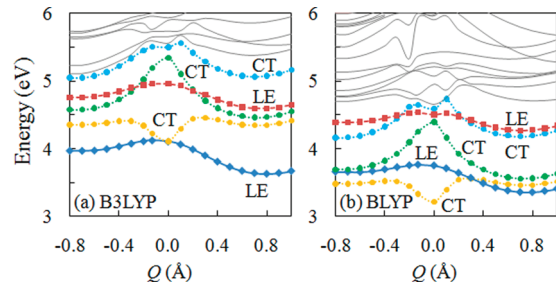


**Figure 7.** Potential energy profiles of the lowest five excited states of the 7AI dimer as functions of the reaction coordinate  $Q$ , calculated at the (a) B3LYP and (b) BLYP levels. Reaction paths are optimized for the lowest LE state with the LC-BLYP method. Ground-state energy of  $ND_{S0}$  is taken as zero. Full line with filled diamonds indicates the energies of the lowest LE state whose geometries are optimized. Dashed lines with filled squares indicate energies of other LE states, while dotted lines with filled circles indicate energies of CT states. Energies of sixth and higher excited states are also shown by thin solid lines.

proton at the  $N1 - H10 \cdots N7'$  hydrogen bond is much closer to monomer-g than monomer-e ( $r_3 = 1.177 \text{ \AA}$ ,  $r_4 = 1.418 \text{ \AA}$ ,  $M_2 = -0.241 \text{ \AA}$ ). A similar feature is found at the geometry of the energy maximum point of the CASPT2 potential energy curve ( $Q = -0.3 \text{ \AA}$ ), where  $r_1 = 1.189 \text{ \AA}$ ,  $r_2 = 1.377 \text{ \AA}$ , and  $M_1 = -0.188 \text{ \AA}$  in the  $N1' - H10' \cdots N7$  hydrogen bond and  $r_3 = 1.104 \text{ \AA}$ ,  $r_4 = 1.516 \text{ \AA}$ , and  $M_2 = -0.421 \text{ \AA}$  in the  $N1 - H10 \cdots N7'$  hydrogen bond. These findings suggest an asynchronous DPT where the proton transfer from monomer-e to monomer-g along the former hydrogen bond is likely to be completed earlier than the proton transfer from monomer-g to monomer-e along the latter hydrogen bond. One point should be noted about the difference between asynchronous reaction (concerted reaction) and stepwise reaction. In asynchronous (concerted) reaction, two protons are transferred in different pace, but no stable SPT intermediate is formed. In stepwise reaction, on the other hand, a stable intermediate is formed after the first SPT. The asynchronous concerted mechanism has also been exhibited in ab initio molecular dynamics simulations of the excited-state hydrogen transfer in clusters of the 7AI monomer with one or two water molecules.<sup>74</sup> A transition state for synchronous ESDPT process with  $C_{2h}$  symmetry [ $TS_{S1}(C_{2h})$ ] was also located by the LC-BLYP method (see the Supporting Information for the optimized structure). The energy of  $TS_{S1}(C_{2h})$  is evaluated as 6.3 kcal/mol higher than  $ND_{LE}$ . The energy barrier indicates that the synchronous ESDPT process is less competitive to take place than the asynchronous ESDPT process, which exhibits a barrier of 1.5 kcal/mol. In addition,  $TS_{S1}(C_{2h})$  exhibits two imaginary frequency modes, so this structure is characterized as a second-order saddle point. One of the imaginary frequency modes is an  $a_g$  mode corresponding to the symmetric proton-transfer motion, while the other is a  $b_u$  mode corresponding to in-plane motion of the rings, which breaks the  $C_{2h}$  symmetry. This finding means that the reaction path of the synchronous ESDPT from  $ND_{S1}(C_{2h})$  to  $TD_{S1}(C_{2h})$  through  $TS_{S1}(C_{2h})$  is unstable with respect to the  $b_u$  imaginary frequency mode (see also Section 3.1).

As for ab initio methods, geometry optimization by the CASPT2 method in the present work has exhibited the concerted mechanism in the LE state and has not located any minima corresponding to a zwitterionic intermediate. Some recent ab initio studies using the CIS or CASSCF method for the geometry optimization, on the other hand, located an excited-state

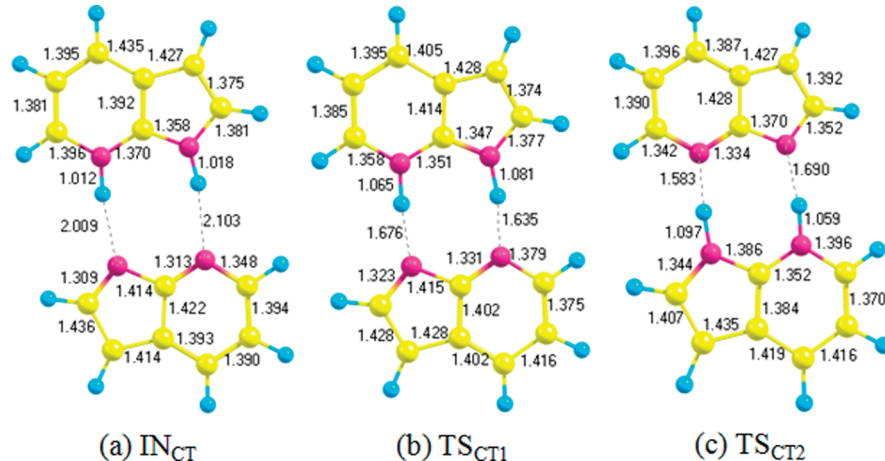


**Figure 8.** Geometries of (a) minimum in the lowest CT state ( $\text{IN}_{\text{CT}}$ ) and (b and c) transition states on reaction paths of stepwise ESDPT through  $\text{IN}_{\text{CT}}$  ( $\text{TS}_{\text{CT}1}$  and  $\text{TS}_{\text{CT}2}$ ) of the 7AI dimer, optimized at the LC-BLYP level. Bond lengths are in angstroms.

minimum for the zwitterionic intermediate.<sup>42,46,49</sup> This discrepancy can be attributed to the lack of dynamic electron correlation in the latter methods. With respect to the CASSCF optimization, it should also be noticed that a minimum for the zwitterionic intermediate was located in one study,<sup>49</sup> while it could not be located in other studies.<sup>4,50</sup> One possible explanation for this difference is that the intermediate minimum located in the former study may be artificial. In ref 49, the minimum of the zwitterionic intermediate is located in the  $S_2$  state at the CASSCF level, while this electronic state changes to  $S_1$  at the CASPT2 level. This change is caused by different contributions from dynamic electron correlation effects in the  $S_1$  and  $S_2$  states. In such a situation, shape of the CASPT2 potential energy surface may be significantly different from the CASSCF potential energy surface,<sup>75</sup> and it is therefore possible that the intermediate minimum at the CASSCF level disappears at the CASPT2 level.

We also applied the conventional TDDFT method with the B3LYP and BLYP functionals (without LC) to calculate the potential energy profiles of 20 lowest excited states along the reaction path optimized by the LC-BLYP method. Figure 7 shows the resulting potential energy curves of low-lying excited states. As is clearly shown here, the energies of CT states are drastically underestimated in both B3LYP and BLYP calculations compared with the LC-BLYP calculations. In the B3LYP calculations (Figure 7a), the lowest CT state corresponding to a charge transfer from monomer-e to monomer-g appears as the second excited state along the reaction path (yellow line). Moreover, the CT state is almost degenerate with the lowest LE state near the maximum point of the ESDPT potential energy curve ( $Q = 0$  Å). In the BLYP calculations (Figure 7b), the first CT state is found to be below the lowest LE state around the  $\text{ND}_{\text{LE}}$  structure and exhibits considerably lower energy near the maximum point. The energy profiles at the B3LYP and BLYP levels are quite different from the LC-BLYP energy profiles calculated along the same reaction path (Figure 5b), where the first CT state is found to be much higher in energy than the lowest four LE states. At the B3LYP and BLYP levels, a large number of excited states are found within the range of less than 6 eV as shown in Figure 7. Note that in the LC-BLYP calculations only the four LE states are found in the same range (see Figure 5b).

The B3LYP method was also used for the optimization of the ESDPT reaction path. The resulting potential energy curve

(shown in the Supporting Information) exhibits a considerably deep minimum of the CT state near  $Q = 0$  due to the large underestimation of the energies of this state. A similar behavior of the ESDPT potential energy curve at the B3LYP level was reported by Catalán and de Paz.<sup>34</sup> The authors calculated the potential energy profiles of the first excited state in  $C_s$  symmetry, resulting in significant energy lowering of intermediate structure and the dissociation of the 7AI dimer. Thus conventional TDDFT methods predict quite a different mechanism of the ESDPT in the 7AI dimer from the LC-TDDFT method as well as from the CASPT2 method.

**3.3. Reaction Path in the Charge-Transfer State.** The stepwise mechanism of the ESDPT via a neutral intermediate in the CT state was also investigated using the LC-BLYP method. Figure 8 shows the optimized geometries of stationary points relevant to the stepwise ESDPT. The minimum in the CT state for the neutral intermediate, labeled as  $\text{IN}_{\text{CT}}$ , has been found in a SPT structure ( $M_1 = 0.997$ ,  $M_2 = -1.085$  Å; see Figure 8a) and with the energy of 4.9 kcal/mol lower than  $\text{ND}_{\text{LE}}$ . At  $\text{IN}_{\text{CT}}$ , the first excited state is a CT state in which electron is transferred from HOMO of the monomer of proton donor to LUMO of the monomer of proton acceptor (see Figure 4 for HOMO and LUMO of the monomer), compensating the positive charge of the transferred proton. The lengths of  $\text{N}1' \cdots \text{H}10'$  and  $\text{N}7' \cdots \text{H}10$  hydrogen bonds (2.009 and 2.103 Å, respectively) are found to be much shorter than the calculated values in previous theoretical studies,<sup>42,46,49</sup> due to the difference of computational methods used for the geometry optimization.

Transition states of SPT structure which may be accessed during the stepwise ESDPT through  $\text{IN}_{\text{CT}}$  have also been located. Figure 8b and c shows two transition-state structures optimized at the LC-BLYP level, referred to as  $\text{TS}_{\text{CT}1}$  ( $M_1 = 0.611$ ,  $M_2 = -0.544$  Å) and  $\text{TS}_{\text{CT}2}$  ( $M_1 = -0.486$ ,  $M_2 = 0.631$  Å), respectively. The transition state  $\text{TS}_{\text{CT}1}$  ( $\text{TS}_{\text{CT}2}$ ) exhibits the energy which is 6.0 kcal/mol (6.9 kcal/mol) higher than  $\text{ND}_{\text{LE}}$  and 10.9 kcal/mol (11.8 kcal/mol) higher than  $\text{IN}_{\text{CT}}$ . When the zero-point energy correction is implemented, the energy difference between  $\text{ND}_{\text{LE}}$  and  $\text{TS}_{\text{CT}1}$  ( $\text{TS}_{\text{CT}2}$ ) is 3.5 kcal/mol (4.3 kcal/mol) and the energy difference between  $\text{IN}_{\text{CT}}$  and  $\text{TS}_{\text{CT}1}$  ( $\text{TS}_{\text{CT}2}$ ) is 7.3 kcal/mol (8.1 kcal/mol). The electronic structure of the  $S_1$  state at these transition states is characterized as mixing of CT and LE configurations, although the monomer exhibiting

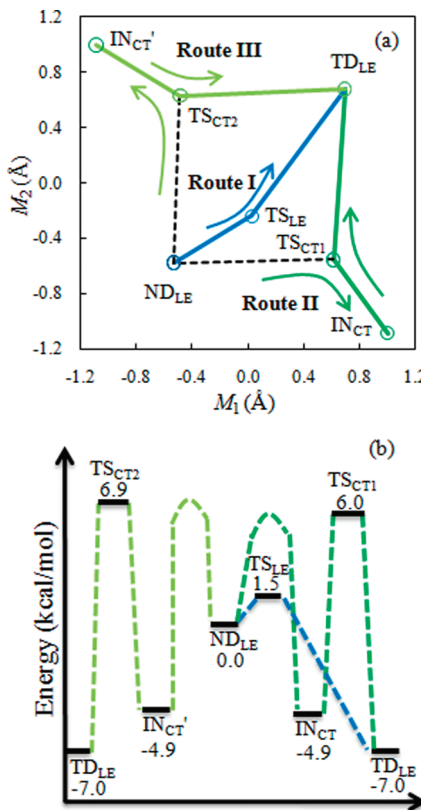


**Figure 9.** Schematic pictures of the reaction paths of the ESDPT in the 7AI dimer. (a) Reaction routes plotted in the ( $M_1, M_2$ ) plane, where  $M_1$  and  $M_2$  are the reaction coordinates defined in Figure 2 and obtained by LC-BLYP optimization; and (b) energy diagram for reaction routes. Energies (relative to  $ND_{LE}$ ) are calculated at the LC-BLYP level.

local excitation is different between  $TS_{CT1}$  and  $TS_{CT2}$ : The LE configuration at  $TS_{CT1}$  and  $TS_{CT2}$  corresponds to the  $^1L_a$  local excitation on the proton-donating monomer and the proton-accepting monomer, respectively. The character of the CT configuration at the transition states is the same as at  $IN_{CT}$ , where electron is transferred from HOMO of the proton-donating monomer to LUMO of the proton-accepting monomer. In other words, proton and electron are transferred from monomer-e to monomer-g at  $TS_{CT1}$ , while they are transferred from monomer-g to monomer-e at  $TS_{CT2}$ . The  $S_2$  state at both  $TS_{CT1}$  and  $TS_{CT2}$  is found to be nearly degenerate with the  $S_1$  state and also characterized as mixing of LE and CT configurations. This suggests that the  $TS_{CT}$  structures are located near the conical intersection and appear as a result of an avoided crossing of the  $S_1$  and  $S_2$  states.

The IRC calculations show that  $TS_{CT1}$  connects  $IN_{CT}$  and  $TD_{LE}$  while  $TS_{CT2}$  connects  $IN_{CT}'$  (inverted structure of  $IN_{CT}$ ;  $M_1 = -1.085$ ,  $M_2 = 0.997$  Å) and  $TD_{LE}$ . This result suggests that  $TS_{CT1}$  and  $TS_{CT2}$  can be accessed during the second SPT from  $IN_{CT}$  (or  $IN_{CT}'$ ) to  $TD_{LE}$ . As to the first SPT process from  $ND_{LE}$ ,  $IN_{CT}$  can be reached if proton and electron are transferred from monomer-e to monomer-g, while  $IN_{CT}'$  can be reached if the transfer occurs in the opposite direction. The second SPT from  $IN_{CT}$  and  $IN_{CT}'$  is characterized by the proton and electron transfer from monomer-g to monomer-e passing through  $TS_{CT1}$  and from monomer-e to monomer-g passing through  $TS_{CT2}$ , respectively. Unfortunately, the transition state connecting  $ND_{LE}$

and  $IN_{CT}$  via an IRC path could not be found in the present calculations. We tried several transition-state searches starting from medium structures between  $ND_{LE}$  and  $IN_{CT}$  as well as between  $ND_{LE}$  and  $IN_{CT}'$  but all the optimizations led to  $TS_{CT1}$  or  $TS_{CT2}$ .

If the first SPT exhibits a barrier whose height is similar to the energy differences between  $TS_{CT1}$  and  $ND_{LE}$  (6.0 kcal/mol) and between  $TS_{CT2}$  and  $ND_{LE}$  (6.9 kcal/mol), then this process would be less likely to occur than the asynchronous concerted DPT in the LE state discussed in Section 3.2, which exhibits a barrier of 1.5 kcal/mol at the LC-BLYP level. Even if the first SPT exhibits a lower barrier, the stepwise ESDPT through  $IN_{CT}$  may still be less likely to be completed, because the second SPT from  $IN_{CT}$  (or  $IN_{CT}'$ ) to  $TD_{LE}$  along the IRC path through  $TS_{CT1}$  (or  $TS_{CT2}$ ) exhibits a much higher barrier of 10.9 (or 11.8) kcal/mol. It may also be possible that the dimer which has arrived at  $IN_{CT}$  (or  $IN_{CT}'$ ) returns to the ground state through internal conversion resulting from small energy differences between the  $S_0$  and  $S_1$  states before the second SPT occurs.<sup>49</sup> This possibility has also been discussed for 2-aminopyridine dimer, another model of DNA base pairs,<sup>57,76</sup> as well as DNA base pairs themselves (guanine-cytosine and adenine-thymine pairs).<sup>77,78</sup>

**3.4. ESDPT Mechanism.** In the preceding sections, three routes have been presented for the ESDPT reaction in the 7AI dimer:

- Route I:  $ND_{LE} \rightarrow TS_{LE} \rightarrow TD_{LE}$  (concerted mechanism).
- Route II:  $ND_{LE} \rightarrow IN_{CT} \rightarrow TS_{CT1} \rightarrow TD_{LE}$  (stepwise mechanism).
- Route III:  $ND_{LE} \rightarrow IN_{CT}' \rightarrow TS_{CT2} \rightarrow TD_{LE}$  (stepwise mechanism).

Figure 9 shows schematic pictures of the reaction routes. Figure 9a plots the value of the reaction coordinates  $M_1$  and  $M_2$  (defined in Figure 2) for minima and transition states relevant to each route, optimized with the LC-BLYP method. The respective points are connected with straight lines. The transition state connecting  $ND_{LE}$  to  $IN_{CT}$  or  $IN_{CT}'$  could not be found in the present calculations, so the pathways for the SPT reactions among these minima are temporarily expressed by dashed lines connecting  $ND_{LE}$  to  $TS_{CT1}$  and  $TS_{CT2}$  for visibility. Figure 9b shows a diagram for the energy profile of each route calculated at the LC-BLYP level.

In Route I, the 7AI dimer in the lowest LE state tautomerizes from  $ND_{LE}$  to  $TD_{LE}$  by concerted DPT, surmounting an energy barrier of 1.5 kcal/mol at  $TS_{LE}$  (the barrier height is estimated to be 0.5 kcal/mol at the CASPT2 level). The ESDPT reaction proceeds asynchronously, where the  $C_{2h}$  symmetry of the dimer is broken. The synchronous ESDPT conserving  $C_{2h}$  symmetry exhibits higher potential energies than the asynchronous ESDPT in  $C_s$  symmetry accompanying the unstable reaction path with respect to the in-plane mode which breaks the  $C_{2h}$  symmetry. In Routes II and III, on the other hand, two SPTs occur sequentially. For Route II, the first SPT from  $ND_{LE}$  to  $IN_{CT}$  forms a neutral intermediate by proton and electron transfer from monomer-e to monomer-g. The second SPT from  $IN_{CT}$  to  $TD_{LE}$  occurs through  $TS_{CT1}$ , overcoming an energy barrier of 10.9 kcal/mol by proton and electron transfer from monomer-g to monomer-e.  $TS_{CT1}$  is 6.0 kcal/mol higher in energy than  $ND_{LE}$ . Similarly, for Route III, the first SPT from  $ND_{LE}$  to  $IN_{CT}'$  forms a neutral intermediate. However, the direction of the proton and electron transfer is opposite to Route II, from monomer-g to monomer-e. For the second SPT from  $IN_{CT}'$  to  $TD_{LE}$ , the dimer has to

overcome an energy barrier of 11.8 kcal/mol at  $\text{TS}_{\text{CT}2}$  by proton and electron transfer from monomer-e to monomer-g.  $\text{TS}_{\text{CT}2}$  is 6.9 kcal/mol higher in energy than  $\text{ND}_{\text{LE}}$ .

According to the energy profiles of the three routes, it seems that the asynchronous concerted mechanism through Route I is the most likely to be followed. In the case of the gas phase, at least, one can say that the ESDPT in the 7AI dimer proceeds with the concerted mechanism at the lowest excitation energy. The stepwise mechanism through Routes II or III may also be possible at higher excitation energies.

In the concerted mechanism, the ESDPT in the 7AI dimer is a single-step process. This is consistent with the single-exponential decay of time-resolved electronic spectra of ND at the lowest excitation energy observed in the gas phase<sup>33</sup> as well as in a nonpolar solvent.<sup>36</sup> Presumably, the biexponential decay of other spectra in the two phases can be explained by combination with another process at higher excitation energy. For the gas phase, ESDPT after vibronic excitation of intermolecular stretching mode may correspond to the faster component of the biexponential decay, as Sakota et al.<sup>33</sup> proposed. In the case of nonpolar solvent, Takeuchi and Tahara<sup>36</sup> assigned the faster decay of fluorescence spectrum to internal conversion from higher to the first electronic excited state.

In the experiments on deuterated compounds of the 7AI dimer, moderate difference was found in the ESDPT rate constant of two isotopomers (one of them is deuterated on the NH group of monomer-e, while the other one is deuterated on the NH group of monomer-g).<sup>32,37</sup> This kinetic isotope effect supports the asynchronous concerted mechanism in  $C_s$  symmetry, where the two SPTs proceed in different pace. If the ESDPT process were a synchronous process where  $C_{2h}$  symmetry is strictly retained, the two rate constants would be the same.

Photochemical behavior of the 7AI dimer can be considerably different in polar solvent. Based on time-resolved fluorescence spectra, Kwon and Zewail<sup>37</sup> proposed that the rate of ESDPT is significantly dependent on the polarity of solvent. On the other hand, Catalán<sup>79</sup> concluded that the 7AI molecule does not form a hydrogen-bonded dimer in polar solvent using steady-state absorption and emission spectroscopy. If the ESDPT occurs also in polar solvent with the asynchronous concerted mechanism presented in this work, then electrostatic interaction between solute and solvent molecules is expected to largely affect the reaction rate, because the dimer exhibits nonzero dipole moment along the reaction path owing to  $C_s$  symmetry. This is in clear contrast to the synchronous mechanism in  $C_{2h}$  symmetry, where the dipole moment of the dimer remains to be zero. To elucidate the mechanism of the excited-state process in polar solvent, however, additional theoretical studies would be necessary taking into account the effect of solvation on the excited-state potential energy surfaces, which is beyond the scope of the present work.

## 4. CONCLUSIONS

The present paper has shown that the ESDPT in the isolated 7AI dimer is likely to follow the concerted mechanism in terms of excited-state potential energy profiles calculated by the CASPT2 and LC-TDDFT methods. Three routes have been presented for the ESDPT reaction paths. In Route I, the DPT reaction takes place in the LE state through a single transition state following the concerted mechanism. The concerted ESDPT process has been found to occur asynchronously in  $C_s$  symmetry rather than synchronously in  $C_{2h}$  symmetry. The energy barrier for this

asynchronous ESDPT process is estimated to be 1.5 kcal/mol at the LC-TDDFT level and 0.5 kcal/mol at the CASPT2 level. In Routes II and III, on the other hand, the DPT reaction takes place via a neutral intermediate in the CT state following the stepwise mechanism, in which two SPTs occur sequentially. Routes II and III show opposite directions of the charge transfer between monomer-e and monomer-g. The second SPT from the intermediate requires to overcome a barrier of 10.9 and 11.8 kcal/mol in Routes II and III, respectively; these barriers are much higher than the barrier for Route I. Meanwhile, the zwitterionic intermediate presented in previous studies could not be reproduced in any routes.

One important point is that ab initio and DFT methods predict the same mechanism of the ESDPT in the LE state by improving each method. In the present calculations, the CASPT2 and LC-TDDFT methods predict very similar structures of stationary points as well as similar potential energy profiles in low-lying excited states for Route I. It is shown that the conventional TDDFT methods without the LC scheme drastically underestimate the energies of CT states, resulting in a wrong picture that many CT states are included in low-lying excited states along Route I. On the other hand, the LC-BLYP method exhibits no CT states in low-lying excited states along Route I and thus reproduces the CASPT2 results very well. Furthermore, CASSCF optimizations of  $\text{ND}_{\text{LE}}$  are found to predict qualitatively different structure from the CASPT2 and LC-TDDFT optimizations, presumably due to mixing of the  $S_0 - ^1\text{L}_a$  and  $S_0 - ^1\text{L}_b$  configurations. This discrepancy indicates that involvement of dynamic electron correlation is decisive in geometry optimizations for a reliable description of ESDPT process in the 7AI dimer.

This work sheds some new light on the long-lasting question about the mechanism of the ESDPT in the 7AI dimer. To explore the present study further, on-the-fly dynamics simulations of the DPT process in the gas phase and polar and nonpolar solvents would be an interesting topic of future studies.

## ■ ASSOCIATED CONTENT

**S Supporting Information.** Optimized structures of  $\text{TS}_{\text{S}0}$ ,  $\text{ND}_{\text{S}1}(C_{2h})$ ,  $\text{TD}_{\text{S}1}(C_{2h})$ , and  $\text{TS}_{\text{S}1}(C_{2h})$ ; and potential energy curve of the  $\text{S}_1$  state optimized at the B3LYP level. This material is available free of charge via the Internet at <http://pubs.acs.org>.

## ■ AUTHOR INFORMATION

### Corresponding Author

\*E-mail: take@sci.hokudai.ac.jp.

## ■ ACKNOWLEDGMENT

This work was supported by a Grant-in-Aid for Scientific Research from the Ministry of Education, Culture, Sports, Science, and Technology. The computations were performed using the Research Center for Computational Science, Okazaki, Japan. X.Y. thanks the China Scholarship Council, and S.Y. thanks the Japan Society for the Promotion of Science for Research Fellowships for Young Scientists. The authors wish to acknowledge contributions from Ai Saito and Daisuke Nakamura in the initial stage of the present study.

## ■ REFERENCES

- (1) *Proton Transfer in Hydrogen-Bonded Systems*; Bountis, T., Ed.; Plenum: New York, 1992.
- (2) Douhal, A.; Lahmani, F.; Zewail, A. H. *Chem. Phys.* **1996**, *207*, 477.
- (3) *Hydrogen-Transfer Reactions*; Hynes, J. T., Klinman, J. P., Limbach, H.-H., Schowen, R. L., Eds.; Wiley-VCH: Weinheim, Germany, 2007.
- (4) Sekiya, H.; Sakota, K. *J. Photochem. Photobiol. C* **2008**, *9*, 81.
- (5) Taylor, C. A.; El-Bayoumi, M. A.; Kasha, M. *Proc. Natl. Acad. Sci. U.S.A.* **1969**, *63*, 253.
- (6) Ingham, K. C.; Abu-Elgheit, M.; El-Bayoumi, M. A. *J. Am. Chem. Soc.* **1971**, *93*, 5023.
- (7) Ingham, K. C.; El-Bayoumi, M. A. *J. Am. Chem. Soc.* **1974**, *96*, 1674.
- (8) El-Bayoumi, M. A.; Avouris, P.; Ware, W. R. *J. Chem. Phys.* **1975**, *62*, 2499.
- (9) Hetherington, W. M., III; Micheels, R. H.; Eisenthal, K. E. *Chem. Phys. Lett.* **1979**, *66*, 230.
- (10) Waluk, J.; Bulska, H.; Pakuła, B.; Sepioł, J. *J. Lumin.* **1981**, *24/25*, 519.
- (11) Bulska, H.; Grabowska, A.; Pakuła, B.; Sepioł, J.; Waluk, J.; Wild, U. P. *J. Lumin.* **1984**, *29*, 65.
- (12) Fuke, K.; Yoshiuchi, H.; Kaya, K. *J. Phys. Chem.* **1984**, *88*, 5840.
- (13) Tokumura, K.; Watanabe, Y.; Itoh, M. *J. Phys. Chem.* **1986**, *90*, 2362.
- (14) Tokumura, K.; Watanabe, Y.; Udagawa, M.; Itoh, M. *J. Am. Chem. Soc.* **1987**, *109*, 1346.
- (15) Fuke, K.; Kaya, K. *J. Phys. Chem.* **1989**, *93*, 614.
- (16) Share, P.; Pereira, M.; Sarisky, M.; Repinec, S.; Hochstrasser, R. M. *J. Lumin.* **1991**, *48/49*, 204.
- (17) Douhal, A.; Kim, S. K.; Zewail, A. H. *Nature* **1995**, *378*, 260.
- (18) Takeuchi, S.; Tahara, T. *Chem. Phys. Lett.* **1997**, *277*, 340.
- (19) Chachisvilis, M.; Fiebig, T.; Douhal, A.; Zewail, A. H. *J. Phys. Chem. A* **1998**, *102*, 669.
- (20) Folmer, D. E.; Poth, L.; Wisniewski, E. S.; Castleman, A. W., Jr. *Chem. Phys. Lett.* **1998**, *287*, 1.
- (21) Takeuchi, S.; Tahara, T. *J. Phys. Chem. A* **1998**, *102*, 7740.
- (22) Fiebig, T.; Chachisvilis, M.; Manger, M.; Zewail, A. H.; Douhal, A.; Garcia-Ochoa, I.; de La Hoz Ayuso, A. *J. Phys. Chem. A* **1999**, *103*, 7419.
- (23) Folmer, D. E.; Wisniewski, E. S.; Hurley, S. M.; Castleman, A. W., Jr. *Proc. Natl. Acad. Sci. U.S.A.* **1999**, *96*, 12980.
- (24) Folmer, D. E.; Wisniewski, E. S.; Castleman, A. W., Jr. *Chem. Phys. Lett.* **2000**, *318*, 637.
- (25) Catalán, J.; Kasha, M. *J. Phys. Chem. A* **2000**, *104*, 10812.
- (26) Takeuchi, S.; Tahara, T. *Chem. Phys. Lett.* **2001**, *347*, 108.
- (27) Catalán, J. *J. Phys. Chem. A* **2002**, *106*, 6738.
- (28) Sakota, K.; Hara, A.; Sekiya, H. *Phys. Chem. Chem. Phys.* **2004**, *6*, 32.
- (29) Catalán, J.; Pérez, P.; del Valle, J. C.; de Paz, J. L. G.; Kasha, M. *Proc. Natl. Acad. Sci. U.S.A.* **2004**, *101*, 419.
- (30) Catalán, J. *Phys. Chem. Chem. Phys.* **2004**, *6*, 4467.
- (31) Sakota, K.; Sekiya, H. *J. Phys. Chem. A* **2005**, *109*, 2718.
- (32) Sakota, K.; Sekiya, H. *J. Phys. Chem. A* **2005**, *109*, 2722.
- (33) Sakota, K.; Okabe, C.; Nishi, N.; Sekiya, H. *J. Phys. Chem. A* **2005**, *109*, 5245.
- (34) Catalán, J.; de Paz, J. L. G. *J. Chem. Phys.* **2005**, *123*, 114302.
- (35) Sekiya, H.; Sakota, K. *Bull. Chem. Soc. Jpn.* **2006**, *79*, 373.
- (36) Takeuchi, S.; Tahara, T. *Proc. Natl. Acad. Sci. U.S.A.* **2007**, *104*, 5285.
- (37) Kwon, O.-H.; Zewail, A. H. *Proc. Natl. Acad. Sci. U.S.A.* **2007**, *104*, 8703.
- (38) Catalán, J. *J. Phys. Chem. A* **2010**, *114*, 5666.
- (39) Pechenaya, V. I.; Danilov, V. I. *Chem. Phys. Lett.* **1971**, *11*, 539.
- (40) Catalán, J.; Pérez, P. *J. Theor. Biol.* **1979**, *81*, 213.
- (41) Waluk, J.; Bulska, H.; Grabowska, A.; Mordziński, A. *Nouv. J. Chim.* **1986**, *10*, 413.
- (42) Douhal, A.; Guallar, V.; Moreno, M.; Lluch, J. M. *Chem. Phys. Lett.* **1996**, *256*, 370.
- (43) Guallar, V.; Batista, V. S.; Miller, W. H. *J. Chem. Phys.* **1999**, *110*, 9922.
- (44) Catalán, J.; del Valle, J. C.; Kasha, M. *Proc. Natl. Acad. Sci. U.S.A.* **1999**, *96*, 8338.
- (45) del Valle, J. C.; Kasha, M.; Catalán, J. *Int. J. Quantum Chem.* **2000**, *77*, 118.
- (46) Moreno, M.; Douhal, A.; Lluch, J. M.; Castaño, O.; Frutos, L. M. *J. Phys. Chem. A* **2001**, *105*, 3887.
- (47) Catalán, J.; Pérez, P.; del Valle, J. C.; de Paz, J. L. G.; Kasha, M. *Proc. Natl. Acad. Sci. U.S.A.* **2002**, *99*, 5799.
- (48) Gelabert, R.; Moreno, M.; Lluch, J. M. *J. Phys. Chem. A* **2006**, *110*, 1145.
- (49) Serrano-Andrés, L.; Merchán, M. *Chem. Phys. Lett.* **2006**, *418*, 569.
- (50) Ando, K.; Kato, S. Construction of The Potential Function for the Excited State Double Proton Transfer Reaction in 7-Azaindole Dimer. In 13th International Congress of Quantum Chemistry, Helsinki, Finland, June 22–27, 2009; p 197.
- (51) Celani, P.; Werner, H.-J. *J. Chem. Phys.* **2000**, *112*, 5546.
- (52) Celani, P.; Werner, H.-J. *J. Chem. Phys.* **2003**, *119*, 5044.
- (53) Tawada, Y.; Tsuneda, T.; Yanagisawa, S.; Yanai, T.; Hirao, K. *J. Chem. Phys.* **2004**, *120*, 8425.
- (54) Chiba, M.; Tsuneda, T.; Hirao, K. *J. Chem. Phys.* **2006**, *124*, 144106.
- (55) Page, C. S.; Olivucci, M. *J. Comput. Chem.* **2003**, *24*, 298.
- (56) Dreuw, A.; Weisman, J. L.; Head-Gordon, M. *J. Chem. Phys.* **2003**, *119*, 2943.
- (57) Sobolewski, A. L.; Domcke, W. *Chem. Phys.* **2003**, *294*, 73.
- (58) Becke, A. D. *Phys. Rev. A* **1988**, *38*, 3098.
- (59) Lee, C.; Yang, W.; Parr, R. G. *Phys. Rev. B* **1988**, *37*, 785.
- (60) Miehlich, B.; Savin, A.; Stoll, H.; Preuss, H. *Chem. Phys. Lett.* **1989**, *157*, 200.
- (61) Roos, B. O.; Andersson, K. *Chem. Phys. Lett.* **1995**, *245*, 215.
- (62) Becke, A. D. *J. Chem. Phys.* **1993**, *98*, 5648.
- (63) Stephens, P. J.; Devlin, F. J.; Chabalowski, C. F.; Frisch, M. J. *J. Phys. Chem.* **1994**, *98*, 11623.
- (64) Hertwig, R. H.; Koch, W. *Chem. Phys. Lett.* **1997**, *268*, 345.
- (65) Noro, T.; et al. Segmented Gaussian Basis Set; Quantum Chemistry Group: Sapporo, Japan; <http://setani.sci.hokudai.ac.jp/sapporo/>. Accessed February 24, 2011.
- (66) Yamamoto, H.; Matsuoka, O. *Bull. Univ. Electro-Commun.* **1992**, *S*, 23.
- (67) Noro, T.; Sekiya, M.; Koga, T. *Theor. Chem. Acc.* **1997**, *98*, 25.
- (68) Noro, T.; Sekiya, M.; Koga, T. *Theor. Chem. Acc.* **2003**, *109*, 85.
- (69) Werner, H.-J.; Knowles, P. J.; Lindh, R.; Manby, F. R.; Schütz, M.; et al. MOLPRO, version 2008.1; University College Cardiff Consultants Limited: Wales, U.K., 2008.
- (70) Schmidt, M. W.; Baldrige, K. K.; Boatz, J. A.; Elbert, S. T.; Gordon, M. S.; Jensen, J. H.; Koseki, S.; Matsunaga, N.; Nguyen, K. A.; Su, S.; Windus, T. L.; Dupuis, M.; Montgomery, J. A., Jr. *J. Comput. Chem.* **1993**, *14*, 1347.
- (71) Ishikawa, H.; Yabuguchi, H.; Yamada, Y.; Fujihara, A.; Fuke, K. *J. Phys. Chem. A* **2010**, *114*, 3199.
- (72) Platt, J. R. *J. Chem. Phys.* **1949**, *17*, 484.
- (73) Serrano-Andrés, L.; Merchán, M.; Borin, A. C.; Stålring, J. *Int. J. Quantum Chem.* **2001**, *84*, 181.
- (74) Kina, D.; Nakayama, A.; Noro, T.; Taketsugu, T.; Gordon, M. S. *J. Phys. Chem. A* **2008**, *112*, 9675.
- (75) Serrano-Andrés, L.; Merchán, M. *J. Mol. Struct. (THEOCHEM)* **2005**, *729*, 99.
- (76) Schultz, T.; Samoylova, E.; Radloff, W.; Hertel, I. V.; Sobolewski, A. L.; Domcke, W. *Science* **2004**, *306*, 1765.
- (77) Sobolewski, A. L.; Domcke, W.; Hättig, C. *Proc. Natl. Acad. Sci. U.S.A.* **2005**, *102*, 17903.
- (78) Perun, S.; Sobolewski, A. L.; Domcke, W. *J. Phys. Chem. A* **2006**, *110*, 9031.
- (79) Catalán, J. *Nature Precedings* **2009**, <http://hdl.handle.net/10101/npre.2009.3089.1; hdl:10101/npre.2009.3089.1>.